Optimization of AC Filter for New Configuration of Single Phase Current Source PV Inverter Using LabVIEW Platform

SAMEER KHADER[1], ABDEL-KARIM DAUD[2]
[1,2]Palestine Polytechnic University,
[1]Power Electronics Research Unit
Department of Electrical Engineering, Hebron, PALESTINE
[1]sameer@ppu.edu, [2]daud@ppu.edu

Abstract: - This paper proposes a new circuit configuration and a control scheme for a single-phase current source inverter with different operational modes. A sine-triangular wave pulse width modulation SPWM technique is applied, where the switching angle of the inverter is optimized through PWM shifting angle. The inverter is implemented using a single boost switch with H-bridge inverter, and a filter. Different configurations of AC filters are applied mainly C, C-L, L-C, and CLC filter, where the waveform analysis has been detailed to obtain pure sinusoidal output voltage and current with minimized total harmonic distortion, loses and high efficiency. The simulations have been done in LabVIEW software to display the harmonic spectrum, output voltages and currents waveforms. From the simulated results, CLC filter presents better results with respect to the output voltage, load and battery currents, where the obtained total harmonic distortion factor is less than 1.67% and with efficiency of 95%. In addition to that, the drawn battery current for this filter configuration has less values comparing with other configurations, which in turn increases the battery lifetime and reduces the thermal and voltage stresses.

Key-Words: - Current Source Inverter, Sinusoidal Pulse Width Modulated (SPWM), Harmonic Decomposition, LabVIEW Simulation, MATLAB Simulation & Multisim Simulation.

1 Introduction

Photovoltaic Solar energy is the most promising sector for sustainable energy in the coming decades and the depletion over time, where intensive growth in manufacturing huge diversity of solar panels aiming at enhancing the photovoltaic performances [1]-[3]. One of the most important component of the solar system is so called power converter which converts the input DC voltage to output alternating AC voltage with predetermined voltage and frequency [4]-[6], these converters are known as Inverters.

Solar inverters found wide spread application in providing the converted energy to the local electric network (Grid), in this case these inverters are called Grid-Tie inverters [7]-[8] aiming at overcoming the power fluctuation and discontinuity of the source. Another type of inverters called off-grid inverters, where they have to energize isolated loads for economic or technical reasons. Recently for realizing stable and regulated energy, delivery hybrid inverters are used that combine's more than one energy source. Generally, Inverters can be categorized into two types such as single-phase inverters and three phase inverters. Inverters are also classified as voltage source inverters (VSI) where the small or negligible reactor is connected in series with voltage supply and current source inverter (CSI) where high inductance is connected in series with voltage supply.

With respect to circuit configuration inverters can be designed as conventional voltage or source inverter with maximum two input voltages or currents, while multilevel inverters have a minimum of three output voltage levels with reduced harmonic content and increased number of switches [9]-[10].

2 The Proposed Circuit

Current source inverters (CSIs) have major advantages such as eliminated short circuit phenomena, simplified filtering requirements, low THD for output voltage and boosting-up capability. Fig. 1 shows a block diagram of photovoltaic (PV) system with CSI.

Pulse width modulation (PWM) inverter techniques are motivated and developed to control the output AC voltage as well as reduce the harmonics by implementing multiple switching within the inverter with a constant dc input voltage. There a variety of PWM techniques: sinusoidal PWM (SPWM), hysteresis band current control PWM, random PWM, space-vector PWM, etc. The SPWM technique is very popular for industrial inverters [9]-[13].

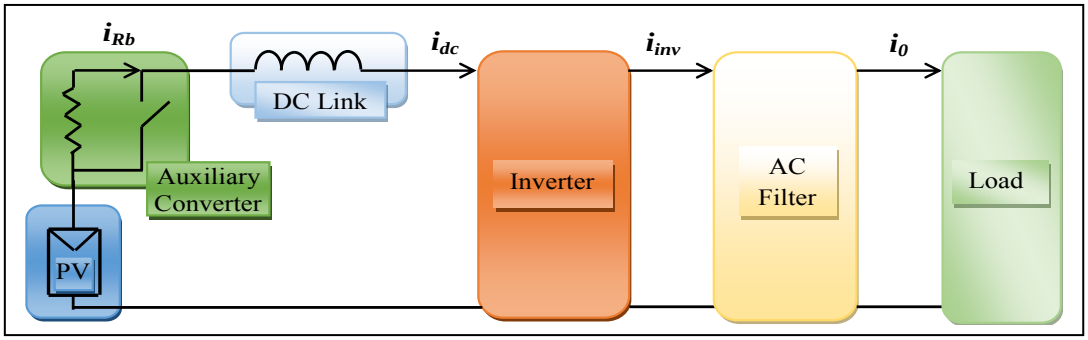

Fig.1 Block diagram of PV system with CSI

The proposed current source inverter with an auxiliary switch and H-bridge inverter with proposed filter configuration as shown in Fig. 2. The proposed topology and its operation are described where the performance of the proposed inverter is predicted by simulation study using LabVIEW software.

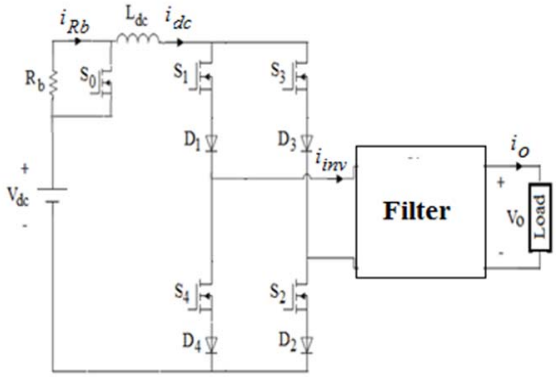

Fig.2 Circuit structure of the proposed PV inverter

The performance of the proposed CSI is optimized for different types of filters as shown in Fig. 3 at different modes of the auxiliary switch of the converter. The optimized factors are:

1) Low THD
2) Reduced heat stress on power source and power switches
3) Reduced the difference between the input and output currents (I_{dc} and I_o)
4) High efficiency and power factor closed to unity.

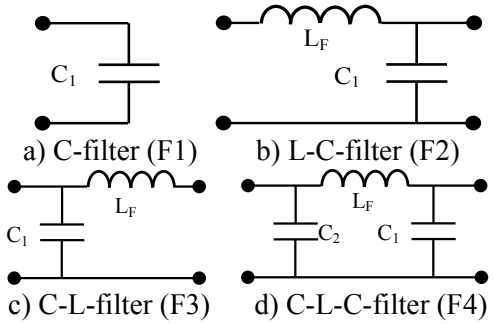

Fig.3 Filters' arrangements

3 System Description

CSI inverters are characterized with one direction flow of the current during conducting mode for this reason there is no need of freewheeling diodes [13],[14]. The proposed CSI is connected to the load via different types of filters as shown in Fig. 2. The switch S_o is used to limit the dc source surge current during the inverter short circuit mode when either S_1 and S_4 or S_2 and S_3 are conducts together. The surge current is limited throughout connecting and disconnecting of the resistance R_b during active (S_0=1) and inactive (S_0=0) switching mode. The DC source (V_{dc}) represents a battery or any renewable energy source with its associate DC/DC converter as input to the CSI. Through the active and inactive of S_0, four switching modes or operation modes for current limiting auxiliary switch S_0 are displayed in Fig. 4.

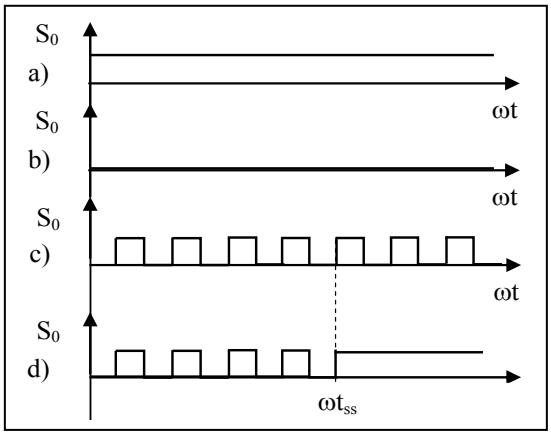

Fig.4 Operation modes of switch $\mathbf{S_0}$ with different values of resistance R_{BC}

a) **Mode A**: $\mathbf{S_0}$ = 1 and R_{BC} = 0 ;
b) **Mode B**: $\mathbf{S_0}$ = 0 and R_{BC} = R_b;
c) **Mode C**: $\mathbf{S_0}$ = 0,1,0,1,0,1,.. and R_{BC} = R_b (1-D_c), where D_c is duty cycle of boost converter
d) **Mode D**: $\mathbf{S_0}$ = 0,1,0,1,0,1,0,1,1,1,1..; R_{BC} = R_b (1-D_c) for t≤ t_{ss} and R_{BC} =0 for t>t_{ss}.

The combination of filter types according to Fig. 3 and different switching modes shown in Fig. 4, the total CSI arrangements are stated in table 1.

Table 1: Different arrangements of CSI

Filter types / Modes of S_0	F1 C-filter	F2 L-C filter	F3 C-L filter	F4 C-L-C filter
A	**A-F1**	**A-F2**	**A-F3**	**A-F4**
B	**B-F1**	**D-F2**	**B-F3**	**B-F4**
C	**C-F1**	**C-F2**	**C-F3**	**C-F4**
D	**D-F1**	**D-F2**	**D-F3**	**D-F4**

The single phase CSI's operation of each arrangement can be divided into four switching states, as illustrated in table 2 under consideration the status of switch S_0 according to figure 4 and table 1 for different CSI arrangements. In table 2, ON-state is depicted by 1 whereas OFF-state is depicted by 0.

As example, the triggering signals for power switches for CSI arrangements for mode C of S_0 can be described as shown in Fig. 5, where the output parameters of CSI depends on the phase shift θ°.

Therefore, by regulating the control shift angle θ°, the main output parameters are regulated as well [15].

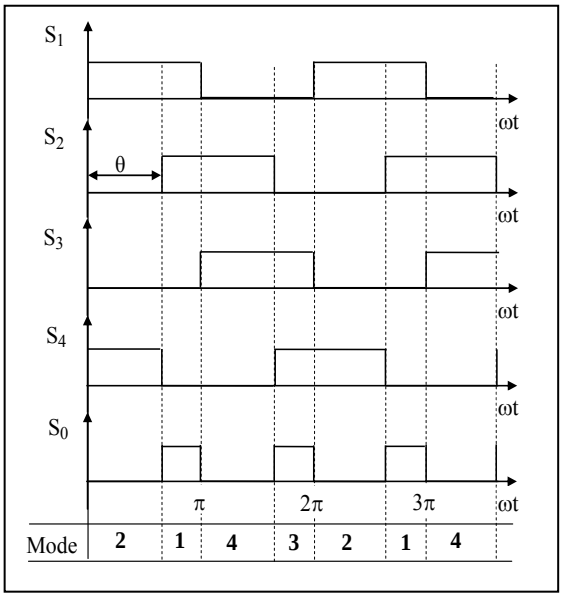

Fig.5 Triggering signals for power switches for CSI arrangements (C-F1, C-F2, C-F3, C-F4).

Table 2. Output current switching pattern for different CSI arrangements

Power Switches / States of Switching	S_0 Modes					S_1	S_2	S_3	S_4	Output current i_o
	A	B	C	D						
				before t_{ss}	after t_{ss}					
1	**1**	**0**	**1**	**1**	**1**	**1**	**1**	**0**	**0**	I_{dc}
2	**1**	**0**	**0**	**0**	**1**	**1**	**0**	**0**	**1**	**0**
3	**1**	**0**	**1**	**1**	**1**	**0**	**0**	**1**	**1**	$-I_{dc}$
4	**1**	**0**	**0**	**0**	**1**	**0**	**1**	**1**	**0**	**0**

3.1 Sinusoidal Pulse Width Modulation

Sinusoidal Pulse Width Modulation (SPWM) technology is used for controlling the proposed inverter as shown on Fig. 6 where the modulation signal v_m is a sinusoidal signal with a frequency of 50 Hz, while the high-frequency triangular carrier signal v_{cr} is generated throughout FPGA clock of 40 MHz, using Lab VIEW software (FPGA – PWM). Therefore, the frequency modulation ratio is very high with 20000 ticks per cycle [16], [17].

The CSI performances can be regulated by changing either the amplitude modulation index M_A or the frequency modulation ratio M_F in order to achieve pure sinusoidal and ripple free output voltage and current at given configuration of the filter topology.

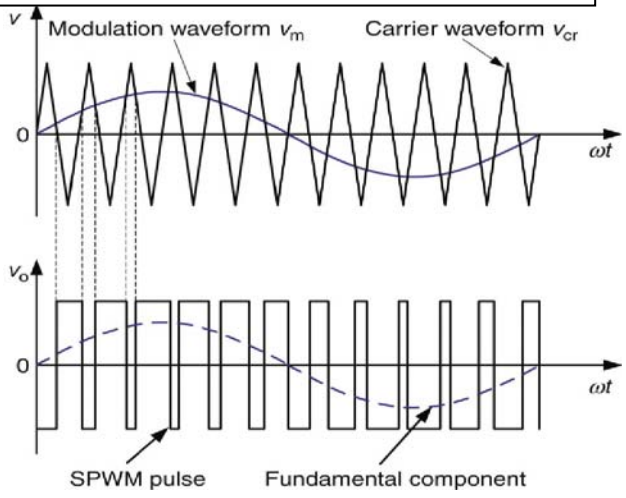

Fig.6 Sinusoidal PWM patterns

3.2 Simulation Tools

The mentioned CSI circuit configurations are simulated using Multisim simulation package [16] in integration with Lab VIEW platform [17], as shown in Fig. 7, while the load and inverter data are stated in table 3.

The simulation results are conducted for different CSI and filters' arrangements according to table 1. The simulation is obtained at optimized switching angle θ, optimized values of the filter parameters C_2 and L_f, and the operation mode of the switch S_0. The optimized switching angle $\theta_{opt}= 168^o$ is selected and applied for simulation of all CSI circuits according to results depicted in [15].

Table 3. PWM and Load Specifications

PWM Generation		Load Data	
Type	FPGA-SPWM	R	10Ω
Clock frequency	40 MHz		
Reference frequency	50Hz		
Amplitude modulation index M_A	0.9		
Pulses/period, Ticks	20000		
Filter data		**CSI data**	
C_1	600uF	R_b	3 Ω
C_2	To be optimized	L_{dc}	600mH
$L_f= L_2$	To be optimized	V_{dc}	36V
		D_1-D_4	1N5406RLG
		Q_1-Q_5 or (S_1- S_4&S_0)	Universal switches

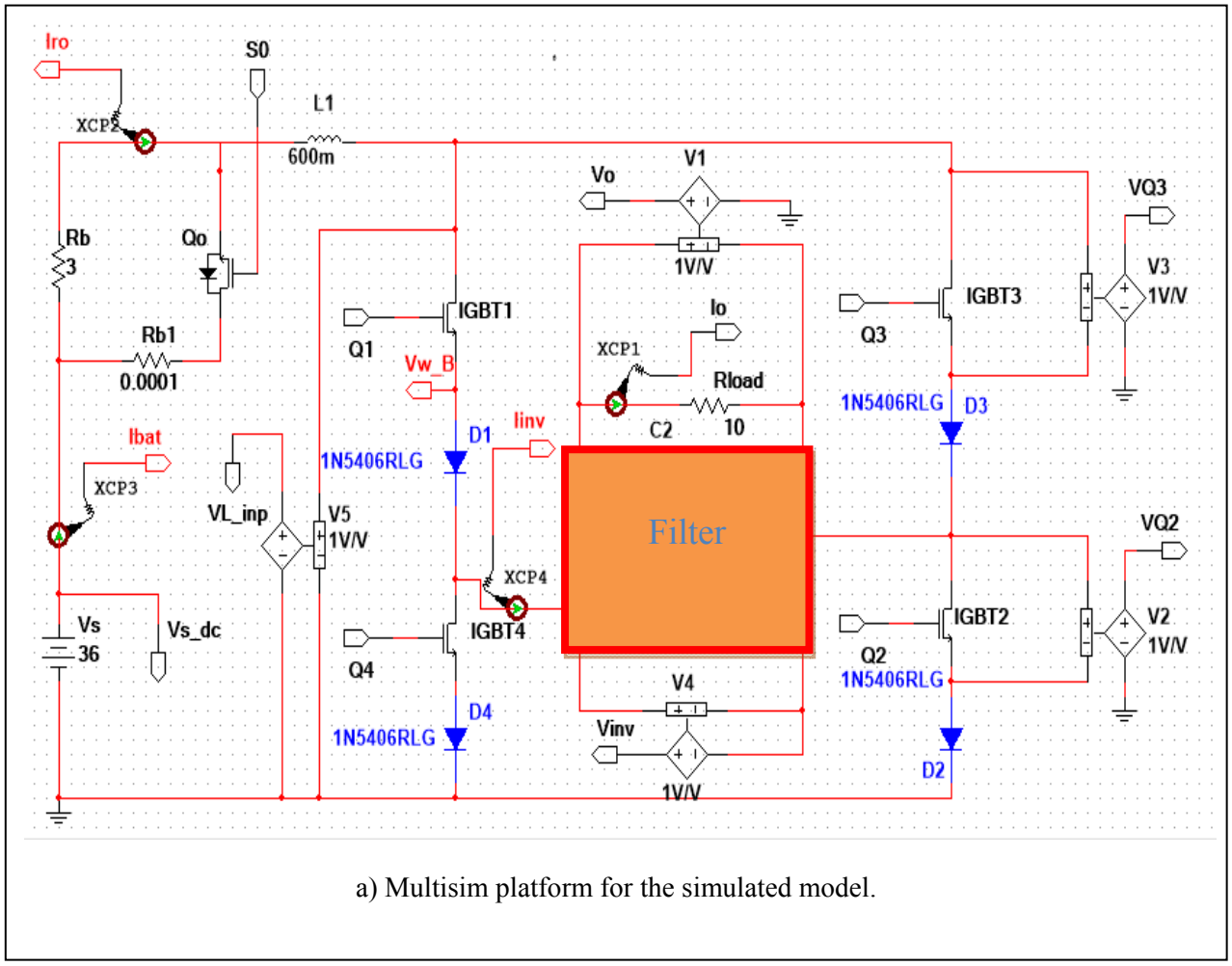

a) Multisim platform for the simulated model.

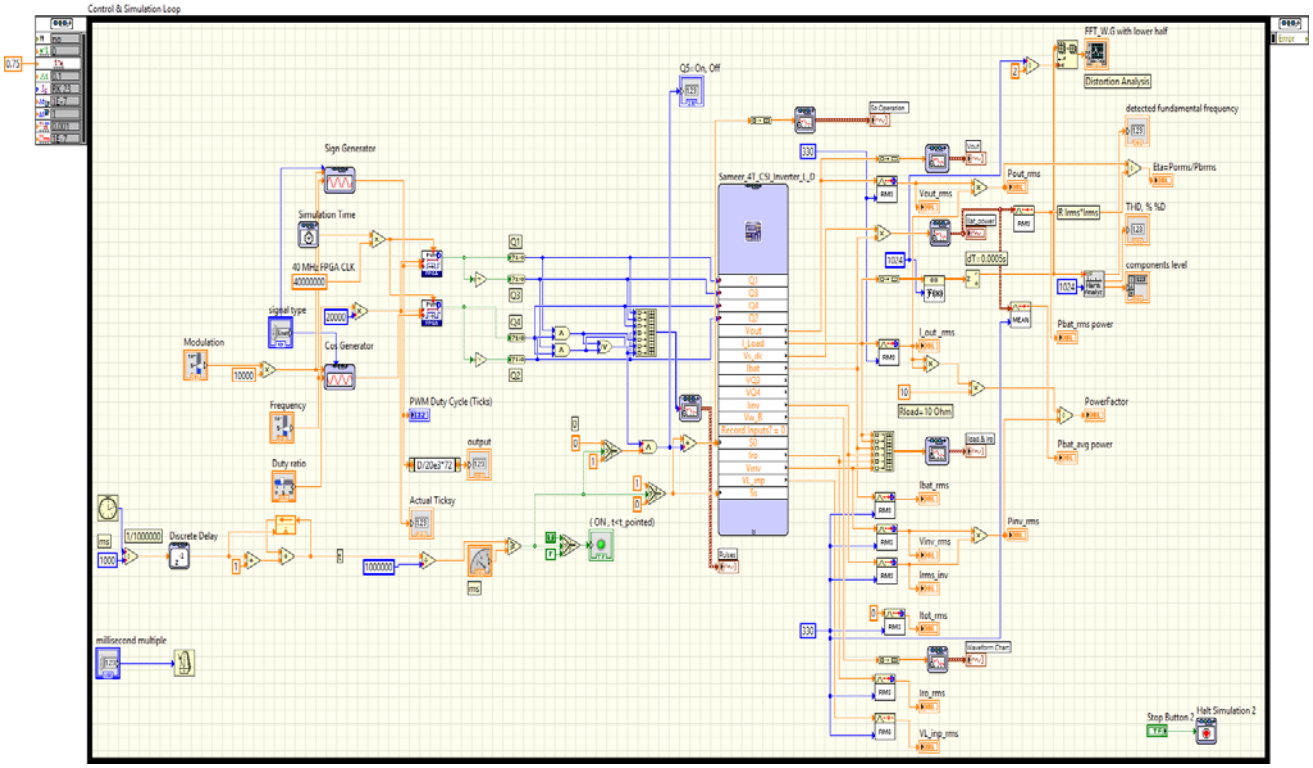

b) LabVIEW platform for the simulated model

Fig.7 Simulation platforms of the proposed model

4. Optimization of CSI Filters' Parameters

Referring to Fig. 3, the values of L_f and C_2 of filters F_2, F_3 and F_4 should be optimized while C_1 is maintained at fixed value of 600µF. Two key parameters are analyzed, the system efficiency and the circuit currents, as follows:

1) The effect of filter's inductance L_f on the circuit currents & efficiency:

While holding C_2 at constant selected value of nearly 300 µF, varying the filter's inductance L_f (L_f =L_2) causes significant change in the efficiency as well shown on Fig. 8(a), where the maximum efficiency approaches it maximum value at optimized value of $L_{f\,opt}$ =41mH. At this value of the inductance, the load and battery currents have closed values as shown on Fig. 8(b), which is good indicator for energy utilization. Furthermore, the proposed filter configuration generates additional energy causing additional current to flow and becomes greater than the inverted current. It noticed that at inductance values greater than $L_{f\,opt}$ the load current exceeds the drawn battery current realizing self-generated phenomena.

2) The effect of filter's capacitance C2 on the circuit currents & efficiency:

While holding L_f at constant value of 41mH, varying the filter's capacitance C_2 causes significant change in the efficiency as shown on Fig. 9 (a), where the maximum efficiency of 95% is achieved at optimized capacitor value of C_{2opt} =276µF .

At this value, the load and battery currents have closed values according to Fig. 9 (b), which is good indicator for energy utilization as well. Furthermore, this present filter's configuration generates additional energy causing additional current to flow greater than the inverted current, where at values greater than C_{2opt} the load current slightly exceeds the drawn battery current. Based on the obtained optimized simulation results the C-L-C filter elements must have C_1=600µF, C_{2opt}=276µF and L_{fopt}=41mH, where these values should serve as reference for the following study and discussions.

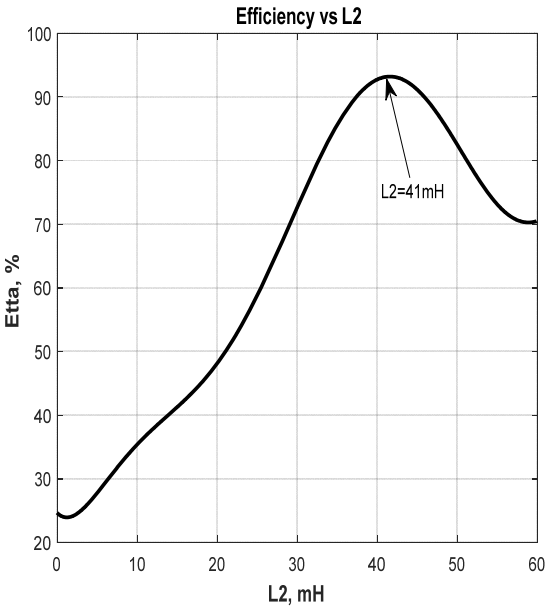

a) System efficiency

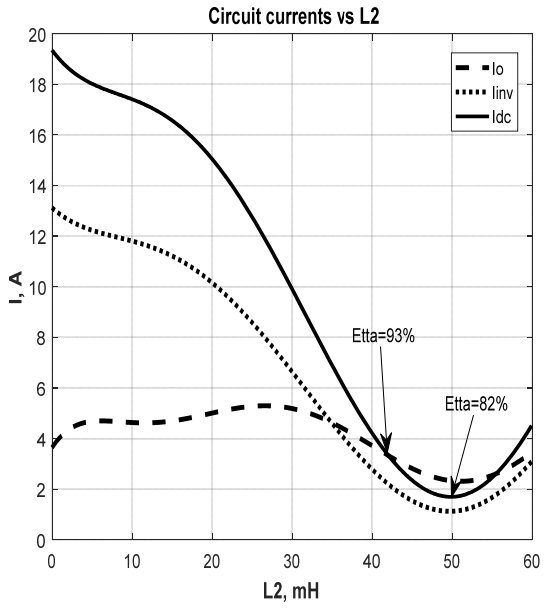

b) Circuit currents

Fig. 8 The effect of filter inductance on the efficiency and currents of C-L-C filter

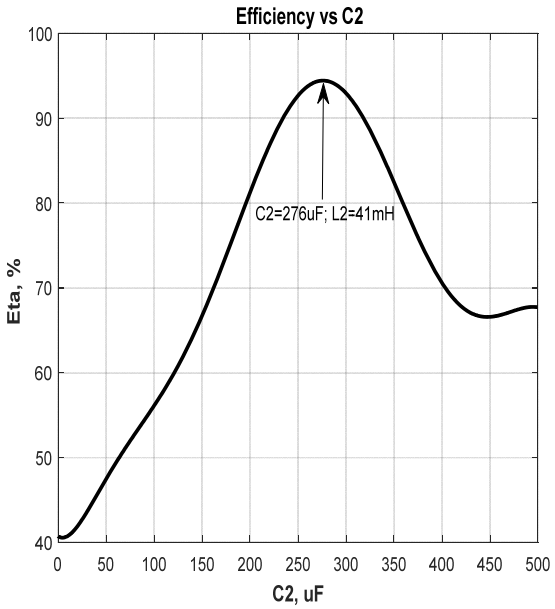

a) System efficiency

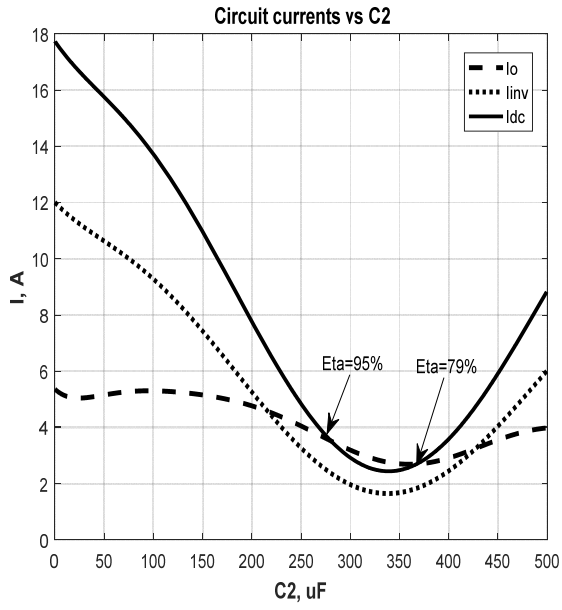

b) Circuit currents

Fig. 9 The effect of filter capacitance C_2 on the efficiency and currents of C-L-C filter

5 Comparison and Optimization of CSI Arrangements

Refer to the CSI arrangements in table 1 and the built simulation models displayed in Fig. 7, table 3 illustrates the performances of CSI circuits for optimized switching angle and optimized filter parameters. Fig. 10 illustrates the load and battery current for all CSI arrangements at different filter types, while Fig. 11 illustrates the most two important quality parameters mainly the distortion factor and the system efficiency.

Referring to these two figures, case D (indexed by D-F4) is characterized with optimized parameters Io=3.59A, I_{dc}=3.69A, η=95%, THD=1.66% and PF closed to unity. The histograms displayed on Fig. 12 shows the comparison analysis between battery and load current for all arrangements and filter types. It noticed that Filter F4 with arrangement (case D) has optimized load current at minimum battery current, which in turn reduces the battery thermal stress, fast discharging and causes long discharging time, which is key indicator for Grid-off PV systems.

Table 3: Performances of different CSI arrangements

Parameter	A-F1	A-F2	A-F3	A-F4	B-F1	B-F2	B-F3	B-F4
I_0, A	5.87	5.27	5.57	3.62	2.04	1.61	1.80	2.71
I_{dc}, A	20.89	25.12	22.64	3.80	7.18	7.70	4.40	2.82
THD, %	2.20	1.61	1.86	2.40	2.0	1.86	1.73	1.79
η, %	46	31	38	93	16	9	12	71
PF	0.52	0.38	0.28	1.0	0.51	0.37	0.27	1.0
Parameter	**C-F1**	**C-F2**	**C-F3**	**C-F4**	**D-F1**	**D-F2**	**D-F3**	**D-F4**
I_0, A	3.01	2.44	2.71	3.12	5.0	4.28	4.60	3.59
I_{dc}, A	10.57	11.68	11.05	3.22	17.63	20.39	18.81	3.69
THD, %	1.74	1.75	1.81	1.8	2.08	1.98	1.75	1.66
η, %	24	14	19	82	39	25	31	95
PF	0.52	0.37	0.28	1.0	0.52	0.37	0.28	1.0

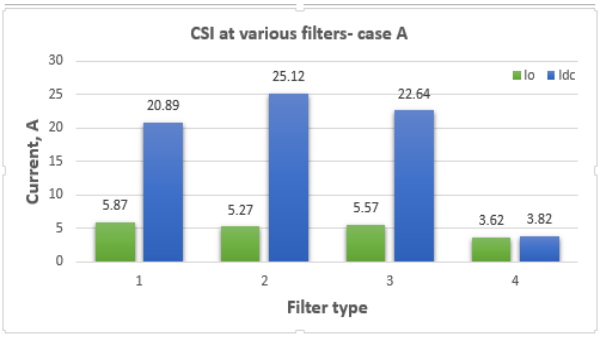

a) Case A arrangement

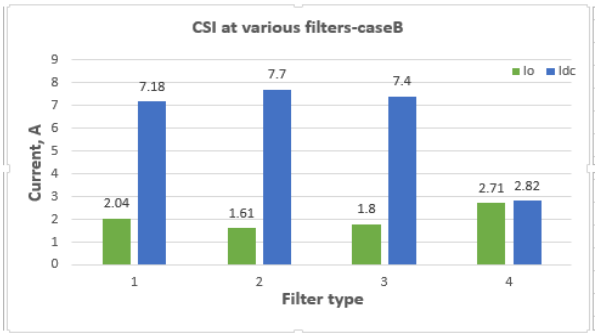

b) Case B arrangement

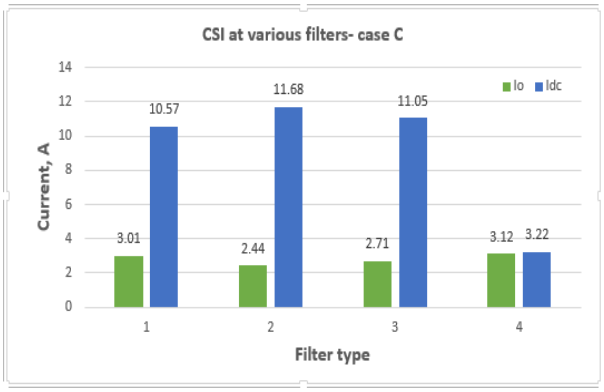

c) Case C arrangement

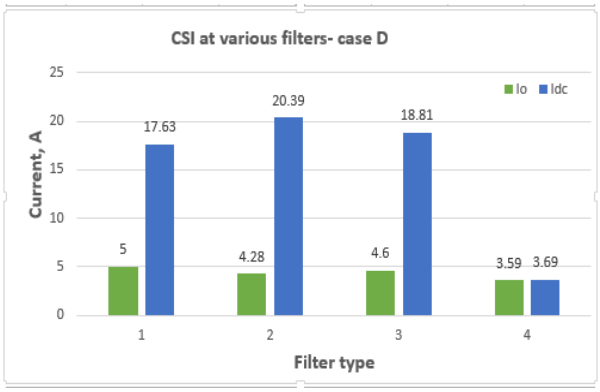

d) Case D arrangement

Fig. 10 Battery and load currents clustered by CSI arrangement at different filter types, where in x-axis 1 means F_1...and 4 means F_4

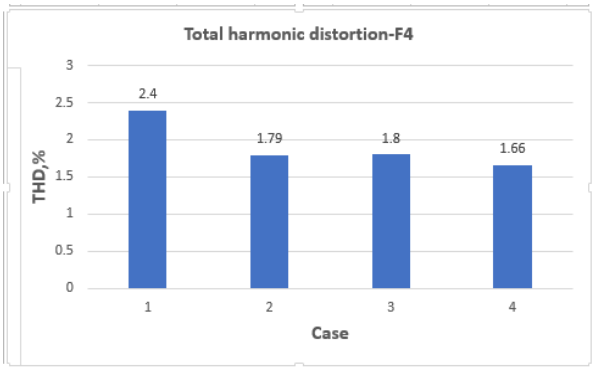

a) Total harmonic distortion

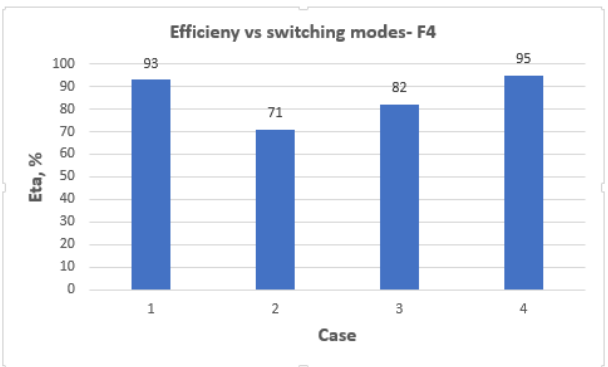

b) System efficiency

Fig. 11 Quality parameters for CSI arrangements at filter type F4

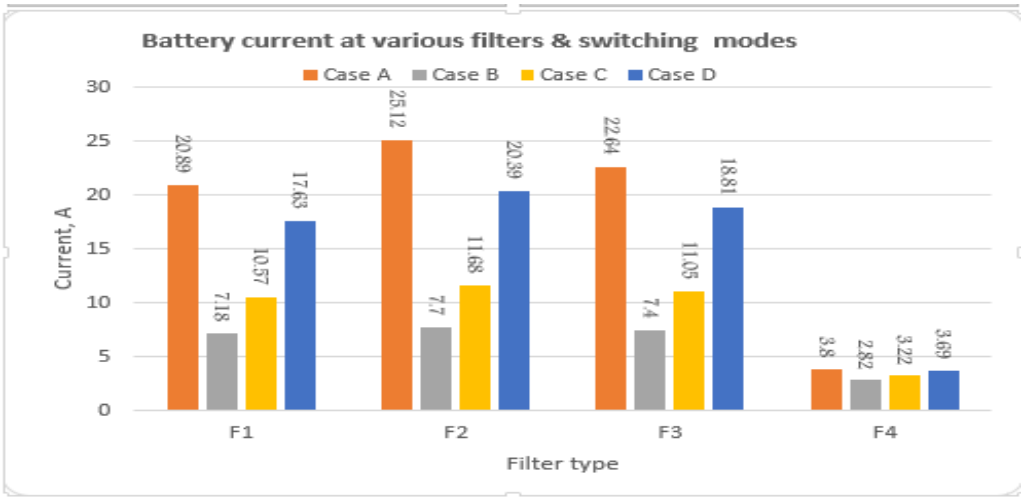

a) Battery current

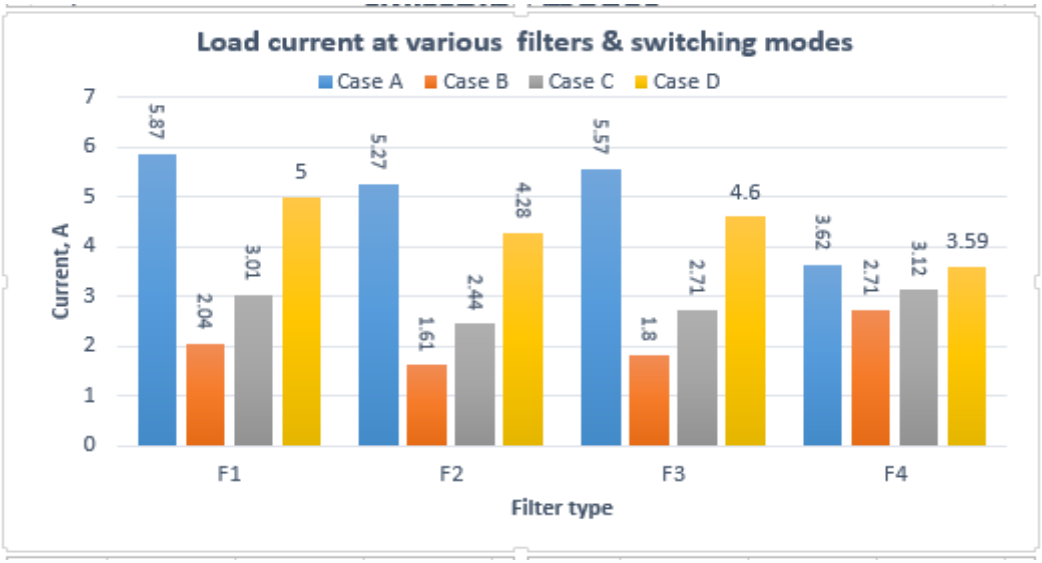

b) Load current.

Fig. 12 Battery and load currents at different CSI arrangements and filter types

6 Displaying of Optimized Proposed CSI Arrangement

Way out from the obtained simulation results displayed in table 3, where the proposed new CSI circuit configurations are described for various switching modes. The CSI arrangement (D-F4) presents the optimized arrangement, while the second arrangement is selected to be (A-F4). Fig. 13 illustrates the front panel and the main circuit parameters of F_1 filter (C-filter) for the optimized switching mode corresponding to case D, [14, 15]. It can be noticed that, there are big differences between the load and battery currents, which in turn causes poor system efficiency of 39%.

The simulation is repeated for the other filter types F_2 and F_3, where the same current and efficiency trends are observed. While it is worthy to study the behaviors of filter F4 presenting C-L-C filter with respect to the drawn current, efficiency and total harmonic distortion.

Fig. 14 illustrates the obtained results for C-L-C filter at optimized certain values of C_1=600µF, C_{2opt}=276 µF and L_{fopt}=41mH, where it can be noticed that, there is negligible difference between battery and load currents, which is good indicator for loss minimization with efficiency of η=95%, and pure sinusoidal performances with THD=1.66%.

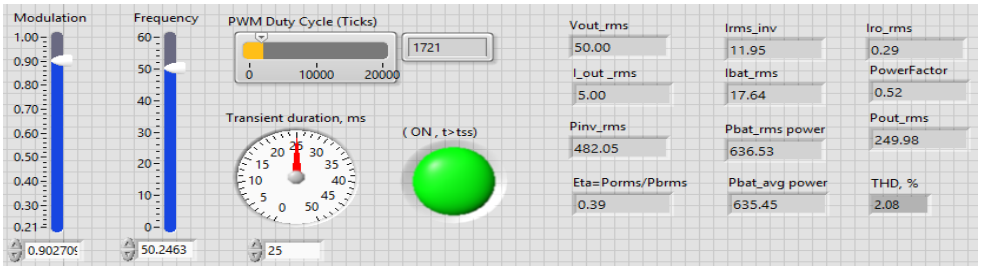

a) Front panel of LabVIEW platform

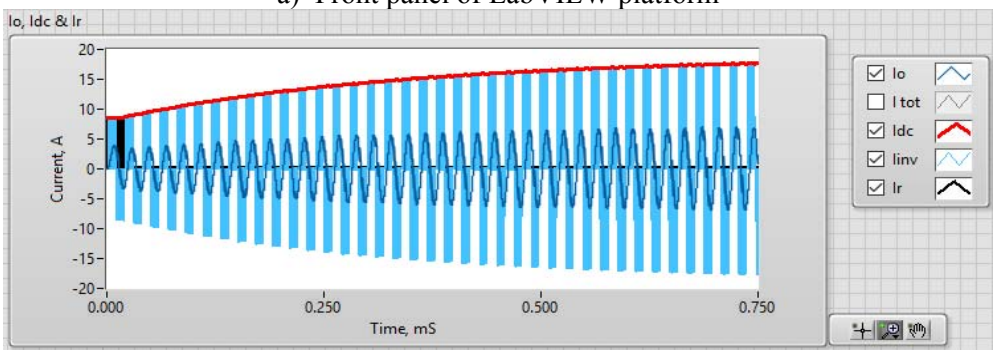

b) Load, inverter and input currents

Fig. 13 LabVIEW front panel and circuit current of C filter and case D

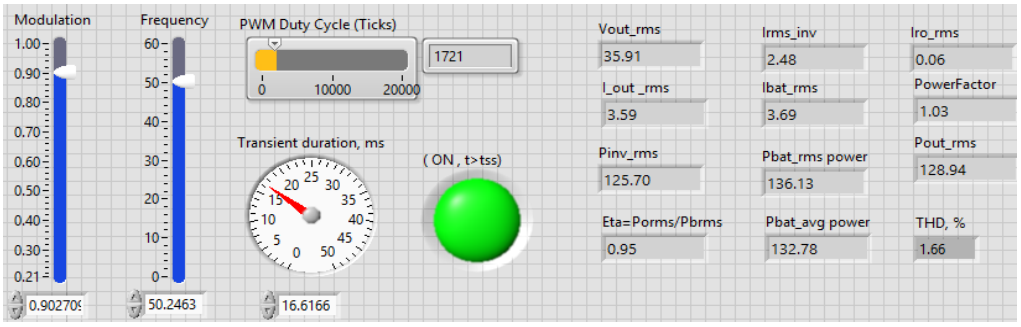

a) Front panel of Lab VIEW platform.

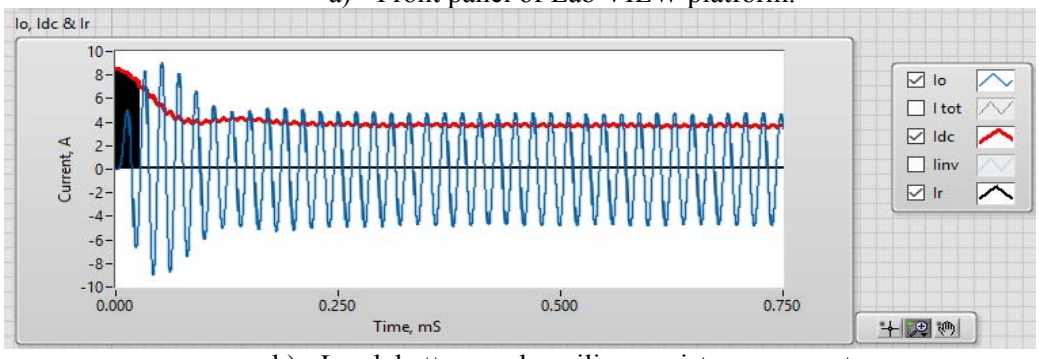

b) Load, battery and auxiliary resistance current

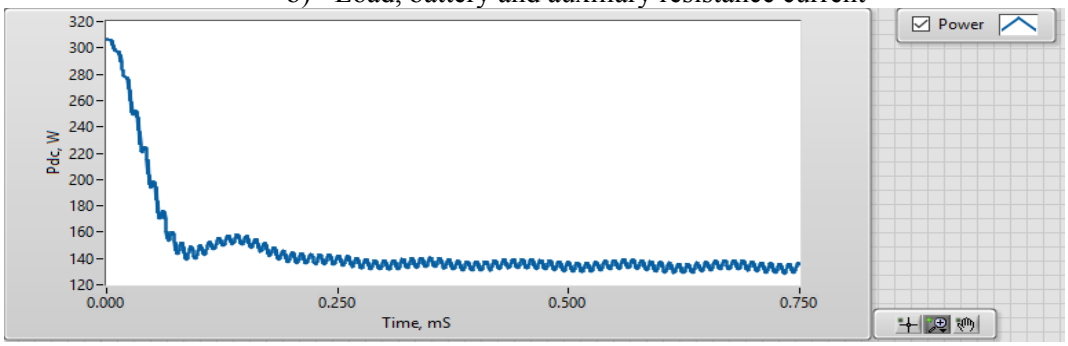

c) Battery power.

Fig. 14 LabVIEW front panel and circuit parameters of C-L-C filter and case D

7 Conclusion

Referring to previous research conducted by the authors [15], which stated that changing the shifting angle between the carrier and reference signal enhances the CSI performance. At given system parameters, it has found that at optimal angle of $\theta_{opt}=168^{\circ}$ the inverter generates pure sinusoidal waveforms with minimized total harmonic distortion and enhanced efficiency. This paper presents the effect of using various filter configurations on the inverter performances at difference switching modes defined as switching modes. Four types of filter configurations were analyzed starting with C, L-C, C-L, and C-L-C filters presented as F_1, F_2, F_3 & F_4 arrangements respectively. The simulation results stated that:

- The optimized CSI performances occur at certain values of C_1, L_f & C_2 , while other values indicates huge loses, great voltage harmonic distortion factor and poor efficiency.
- There is a slight difference between the load and battery current for C-L-C filter in all CSI switching modes, while this difference becomes huge for the rest of filter types, which in turn causes fast battery discharging, and poor system efficiency.
- With respect to load current, case D realizes high drawn efficient current with negligible difference with respect to battery current, in addition to realizing high efficiency and low THD factor.

Finally, combination of optimized switching angle and optimized C-L-C filter values presents unique solution for designing a single-phase CSI inverter with high quality parameters.

References:

[1] M. Calais, J. Myrzik, T. Spoone, and V. G. Agelidis, "Inverters for single-phase grid connected photovoltaic systems-an overview," inProc. 2002 IEEE 33rd Annual Power Electronics Specialists Conference, pesc 02, vol. 2, pp. 1995–2000, 2002.

[2] S. Kjaer and J. Pedersen, "A review of single-phase grid-connected inverters for photo-voltaic modules," IEEE Trans. Ind. Ap., vol. 41,no. 5, pp. 1292-1306, 2005.

[3] S. Khader, A.K. Daud, "PHOTOVOLTAIC-GRID INTEGRATED SYSTEM", First International Conference on Renewable Energies and Vehicular Technology (REVET 2012) Nabeul, Tunisia, pp. 60-65, 2012.

[4] A. K. Daud, M. Mahmoud, "Solar powered induction motor-driven water pump operating on a desert", Renewable Energy, April 2005, Vol. 30, pp. 701-714.

[5] A. K. Daud, M. Ismail, W. Kukhun, M. Mahmoud, "Simulation of a Hybrid Power System Consisting of Wind Turbine, PV, Storage Battery and Diesel Generator: Design, Optimization and Economical Evaluation", International Journal of Energy Engineering (IJEE) Vol.1, No.1, pp.56-61, 2011.

[6] S. Khader, A. K. Daud, "PV-Grid Tie System Energizing Water Pump", Smart Grid and Renewable Energy (SGRE), ISSN Print**:** 2151-481X, Vol. 4, No. 5, pp. 409-418, 2013.

[7] M. H. Rashid, Power Electronics, Devices, Circuits, and Applications, 4th edition, Pearson Education Limited 2014.

[8] M. H. Rashid, Electric Renewable Energy Systems, Academic Press of Elsevier 2016.

[9] H. Komurcugil, "Steady-State Analysis and Passivity-Based Control of Single-Phase PWM Current-Source Inverters," Industrial Electronics, IEEE Transactions on, vol.57, no.3, pp.1026-1030, 2010.

[10] R.T.H. Li, H. S.H. Chung, T.K.M. Chan, "An Active Modulation Technique for Single-Phase Grid-Connected CSI," Power Electronics, IEEE Transactions on, vol.22, no.4, pp.1373-1382, July 2007

[11] Masri and P. W. Chan, "Design and development of a dc-dc Boost converter with constant output voltage", IEEE, International conference on Intelligent and Advanced systems (ICIAS), June 2010.

[12] A. Ponniran and A. F. Said., "DC-DC Boost Converter Design for Solar Electric System", International conference on Instrumentation, Control and Automation, October 20-22 (ICA 2009) Bandung.

[13] R . Arulmurugan, N.V. Suthanthira," Optimal Design of DC to DC Boost Converter with Closed Loop Control PID Mechanism for High Voltage Photovoltaic Application ", International Journal of Power Electronics and Drive System (IJPEDS) Vol.2, No.4, pp. 434-444, December 2012.

[14] A. Nami, A. Ghosh, and F. Blaabjerg, "A hybrid cascade converter topology with series-connected symmetrical and asymmetrical diode-clamped H-Bridge cells", IEEE Trans. Power Electron, vol. 26, no. 1, 51–65, Jan. 2011.

[15] Abdel-Karim Daud, Sameer Khader, " A New Design of Single-Phase Current Source PV Inverter with Load Variation Using Lab View Platform", International Journal of Innovations

in Engineering and Technology (IJIET) , Volume 13 Issue 2 May 2019, pp 3-14.
[16] Multisim Simulation Platform, 14.1 ed., http://www.ni.com/en-us/multisim 14.1.
[17] LabVIEW Simulation Platform, 16 ed., http://www.ni.com/en-us/shop/labview.
[18] Matlab/Simulink User's Guide , 2016, www.mathwork.com